

EARLY-TIME OBSERVATIONS OF THE GRB 050319 OPTICAL TRANSIENT

R. M. QUIMBY,¹ E. S. RYKOFF,² S. A. YOST,² F. AHARONIAN,³ C. W. AKERLOF,² K. ALATALO,^{2,4}
M. C. B. ASHLEY,⁵ E. GÖĞÜŞ,⁶ T. GÜVER,⁷ D. HORNS,³ R. L. KEHOE,⁸ Ü. KUZLUĞLU,⁹
T. A. MCKAY,² M. ÖZEL,¹⁰ A. PHILLIPS,⁵ B. E. SCHAEFER,¹¹ D. A. SMITH,¹²
H. F. SWAN,² W. T. VESTRAND,¹³ J. C. WHEELER,¹ AND J. WREN¹³

Received 2005 October 2; accepted 2005 November 14

ABSTRACT

We present the unfiltered ROTSE-III light curve of the optical transient associated with GRB 050319 beginning 4 s after the cessation of γ -ray activity. We fit a power-law function to the data using the revised trigger time given by Chincarini and coworkers, and a smoothly broken power-law to the data using the original trigger disseminated through the GCN notices. Including the RAPTOR data from Woźniak and coworkers, the best-fit power-law indices are $\alpha = -0.854 \pm 0.014$ for the single power-law and $\alpha_1 = -0.364_{-0.019}^{+0.020}$, $\alpha_2 = -0.881_{-0.031}^{+0.030}$, with a break at $t_b = 418_{-30}^{+31}$ s for the smoothly broken fit. We discuss the fit results, with emphasis placed on the importance of knowing the true start time of the optical transient for this multip peaked burst. As *Swift* continues to provide prompt GRB locations, it becomes more important to answer the question, “when does the afterglow begin?” in order to correctly interpret the light curves.

Subject heading: gamma rays: bursts

1. INTRODUCTION

The precise localization and prompt dissemination of γ -ray bursts (GRBs) from *Swift* has opened the very early time domain of GRB afterglows to exploration. Prior to *Swift*, the few bursts with early afterglow detections engendered an assumption that bright optical flashes commonly dominated the early light curves; however, the growing sample of *Swift* bursts shows, contrary to these expectations, that this phenomenon is rare, and in fact many early light curves show a deficit in flux compared to a backward extrapolation of late-time behavior. GRB 050319 adds to the growing sample of such bursts with early-time optical observations and defines new challenges to interpretation.

The position of GRB 050319 (*Swift* trigger 111622) was distributed as a Gamma-ray Burst Coordinates Network (GCN) notice on 2005 March 19 at 09:31:38 UT, with a 4' radius error box. The notice was issued after a single fast rise exponential decay (FRED) profile triggered the BAT at 09:31:18.44 UT (t_{tr1}); however, Chincarini et al. (2005) report that reanalysis of the prompt BAT light curve reveals the burst actually began 137 s earlier ($t_{\text{tr0}} = t_{\text{tr1}} - 137$ s), but this occurred during a slew, so no alert was issued. Cusumano et al. (2006) give the starting time for GRB 050319 as 09:29:02.70. The BAT light curve thus consists of several peaks with combined $T_{90} = 149.6 \pm 0.7$ s and a 15–350 keV fluence of 1.6×10^{-6} ergs cm^{-2} . There are two principal peaks in the γ -ray light curve; the last peak alone had a 7.3×10^{-7} ergs cm^{-2} fluence and $T_{90} = 23.5$ (Chincarini et al. 2005).

The *Swift* X-Ray Telescope (XRT) began observations of the afterglow at 9:32:45.53 UT (Krimm et al. 2005). Adopting $t_0 = t_{\text{tr0}}$ as the starting point for the afterglow, Chincarini et al. (2005) find an initial steep decline in the X-ray light curve, with a power-law index of $\alpha_1 = -7.64 \pm 3.83$, which breaks at 329 s to $\alpha_2 = -0.50 \pm 0.08$, and a second break to $\alpha_3 = -2.07 \pm 0.06$ that occurs at $t_{\text{tr0}} + 20.5$ hr, where all values are from their first fitting method. Cusumano et al. (2006) give the slopes as $\alpha_1 = -5.53 \pm 0.67$, $\alpha_2 = -0.54 \pm 0.04$, and $\alpha_3 = -1.14 \pm 0.2$, with breaks at 384 ± 22 s and 7.2 ± 1.9 hr, and suggest that the initial fast decay may represent the low-energy tail from the prompt emission. Fynbo et al. (2005) report strong absorption lines in the optical spectra, indicating a redshift of $z = 3.24$.

In this paper, we report on the early-time optical observations of GRB 050319 with the ROTSE-IIIb (Robotic Optical Transient Search Experiment) telescope located at McDonald Observatory, Texas. The observations are described in § 2, and the reduction of the data is detailed in § 3. In § 4 we present power-law function fits to the light curves, exploring both t_{tr0} and t_{tr1} as the start of the optical emission. We end in § 5 with a discussion of the starting time and implications of the multip peaked burst.

¹ Department of Astronomy, University of Texas, Austin, TX 78712; quimby@astro.as.utexas.edu, wheel@astro.as.utexas.edu.

² University of Michigan, 2477 Randall Laboratory, 450 Church Street, Ann Arbor, MI 48104; erykoff@umich.edu, akkerlof@umich.edu, kalatalo@umich.edu, tamckay@umich.edu, hswan@umich.edu, sayost@umich.edu.

³ Max-Planck-Institut für Kernphysik, Saupfercheckweg 1, 69117 Heidelberg, Germany; Felix.Aharonian@mpi-hd.mpg.de, horns@mpi-hd.mpg.de.

⁴ Astronomy, 601 Campbell Hall, University of California, Berkeley, CA 94720; kalatalo@berkeley.edu.

⁵ School of Physics, Department of Astrophysics and Optics, University of New South Wales, Sydney, NSW 2052, Australia; mcba@phys.unsw.edu.au, a.phillips@unsw.edu.au.

⁶ Sabanci University, Orhanlı-Tuzla 34956, Istanbul, Turkey; ersing@sabanciuniv.edu.

⁷ Istanbul University Science Faculty, Department of Astronomy and Space Sciences, 34119, University of Istanbul, Turkey; tolga@istanbul.edu.tr.

⁸ Department of Physics, Southern Methodist University, Dallas, TX 75275; kehoe@physics.smu.edu.

⁹ Middle East Technical University, 06531 Ankara, Turkey; umk@astroa.physics.metu.edu.tr.

¹⁰ Çanakkale Onsekiz Mart Üniversitesi, Terzioğlu 17020, Çanakkale, Turkey; m.e.ozel@ibu.edu.tr.

¹¹ Department of Physics and Astronomy, Louisiana State University, Baton Rouge, LA 70803; schaefer@lsu.edu.

¹² Guilford College, 5800 West Friendly Avenue, Greensboro, NC 27410; dsmith4@guilford.edu.

¹³ Los Alamos National Laboratory, NIS-2 MS D436, Los Alamos, NM 87545; vestrاند@lanl.gov, jwren@nis.lanl.gov.

2. OBSERVATIONS

The ROTSE-III array is a worldwide network of four 0.45 m robotic, automated telescopes, built for fast (~ 6 s) responses to GRB triggers from satellites such as *Swift*. They have a wide ($1^\circ 85 \times 1^\circ 85$) field of view imaged onto a Marconi 2048 \times 2048 back-illuminated thinned CCD, and operate without filters. The ROTSE-III systems are described in detail in Akerlof et al. (2003).

ROTSE-IIIb responded automatically to the GCN notice in under 8 s, with the first exposure starting at 09:31:45.5 UT, just 4 s after the cessation of γ -ray activity. The automated scheduler began a program of ten 5 s exposures, ten 20 s exposures, and 149 60 s exposures before the burst position dropped below our elevation limit. Strong winds introduced tracking errors, which degraded the quality of the initial images. Near real-time analysis of the ROTSE-III images identified a 16th magnitude fading source at $\alpha = 10^h 16^m 47^s.9$, $\delta = +43^\circ 32' 54''.5$ (J2000.0) that was not on the Digitized Sky Survey red plates, which we reported via the GCN Circulars within 25 minutes of the burst (Rykoff et al. 2005). Scattered clouds began to reduce the transparency starting 22 minutes into the response. After 84 minutes the clouds thickened, and the remaining images are not usable.

3. ANALYSIS

The raw ROTSE-III images were processed by an automatic script to eliminate the dark current, and were normalized using a flat field constructed from twilight exposures. We then performed relative photometry on the optical transient (OT) and nearby objects using RPHOT, a custom interactive program implemented in IDL and based around the DAOPHOT routines (Stetson 1987) ported to IDL by Landsman (1989). RPHOT measures both circular aperture and PSF-fit fluxes for objects and provides checks to determine which method produces the best results based on the derived photometric precision of field stars.

We first constructed a deep co-added frame to serve as a reference for both the photometry and the astrometry. The OT is well detected ($S/N > 10$) on the reference image (REFIM). A set of fiducial reference stars (REFSTARS) was chosen from the REFIM to identify nearby ($< 12'$), isolated stars that were not flagged as either saturated or blended by SExtractor (Bertin & Arnouts 1996). An initial list is generated automatically, and remaining sources that appear to deviate from the stellar PSF are removed by hand. The 57 REFSTARS selected are used to derive magnitude zero points relative to the REFIM.

To determine the sky value local to each object under consideration, we calculate a Gaussian-weighted asymmetric clipped mean of the pixels in an annulus of $2r$ to $3r$, where r is 3.5 pixels or the local FWHM, whichever is larger. The calculation is iterative, and pixels 5σ below the mean and the adjacent pixels are rejected, where σ is the current estimate of the Gaussian width. Initially, pixels 3σ above the mean and their neighbors are also rejected, and this clipping threshold is raised with each successive iteration. In addition, the OT sky annulus is given special consideration; using the deep REFIM, all detected sources in the OT sky annulus are masked, and this mask is propagated to the other images. When a preexisting mask is used, clipping is still performed, but with higher initial tolerances. When a large fraction of the sky annulus is masked, it is enlarged to ensure that the formal error in the local sky calculation remains low.

With the OT and reference stars selected and any sky mask set, RPHOT steps through the images and displays the full ac-

tive region, a rectangular area that encompasses the OT and all of the REFSTARS, and a close-up of the OT and its sky annulus. We looked for any global or local problems that might interfere with the photometry. As each image is displayed, RPHOT matches the REFSTARS up to the REFIM using the R.A., decl. solution generated from objects identified by SExtractor. The matched REFSTARS are then used to determine the coordinate mapping from the REFIM. Outliers are rejected from the final solution, and later their positions are recalculated using the final transformation. When few of the REFSTARS are detected on an image due to short exposure times and/or poor weather, the solution based on the full frame is used if the transformation residuals are smaller. The median transformation residuals for these data are typically ~ 0.1 pixels. This transformation is then used to map the OT location as found on the REFIM to each image.

Once the OT and the reference stars have been located on a given image, aperture photometry is performed in a series of concentric, circular apertures ranging from 0.4 to 2.0 times the local FWHM of the image. In addition, a 3.5 pixel ($11''.4$) fixed aperture was used. The local sky values and standard deviations are set using the sky annuli and weighting as described above. RPHOT calculates the weighted average of flux ratios of the reference stars to the REFIM in each aperture in order to derive the relative magnitude offsets.

We finally use the standard DAOPHOT routines to calculate the PSF-fit fluxes. As the PSF does vary significantly across the detector, we selected well-detected objects on each image within $14'$ of the OT to construct the PSF fitting template; this radius represents a balance between improved template accuracy gained from an increase in the number of objects included, and deviations from the OT's PSF at larger separations, which degrade the template. We did not modify the DAOPHOT routines to fix the object centroids for PSF fitting, but allowed them to move as the fitting required, although measurements for which the centroid moved by more than 0.75 times the local FWHM were discarded.

The magnitude scale is set in an absolute sense by calibrating reference stars on the REFIM to a given system. The ROTSE-III telescopes operate without a filter, and the peak sensitivity falls in the R band. We calibrated the magnitude scale using 14 REFSTARS with R -band values determined by Henden (2005), and denote these magnitudes as C_R . The stars used for calibration have colors in the range $0.3 < V - R < 1.0$, with a median of 0.54. Our C_R magnitudes may differ from the R -band values if the spectral energy distribution of the OT differs from that of the median reference star. We can estimate this offset by adopting a blackbody with an effective temperature of 5560 K for our median reference star, and by assuming that the OT spectrum can be represented by $F_\nu \propto \nu^\beta$, with $-1.5 < \beta < -0.5$. With these assumptions, the unfiltered to R -band flux ratio is greater for the OT than for the median reference star, which makes the C_R values 0.1–0.2 mag brighter than the true R -band magnitudes. The correction factor, however, is sensitive to the amount of absorption along the line of sight, as the measured redshift for the OT ($z = 3.24$) places rest-frame Ly α within our bandpass. Depending on the amount of absorption, this could then make the C_R values up to 0.3 mag fainter than the true R -band magnitudes. Note also that we have not corrected our C_R magnitudes for extinction.

RPHOT includes tools to assess the data quality and check the consistency of the relative photometry via the REFSTARS after all the images are processed. The reference stars were all found to have flat light curves, and no trends were found for objects near the OT.

RPHOT initially displays only the S/N for the OT. This is to allow for a co-addition scheme for the later data, when the OT has faded to near or below the individual image limiting magnitudes to be investigated, without biasing the shape of the light curve. This allows us to devise a co-addition scheme for the later data, in which the OT has faded to near or below the limiting magnitudes of the individual images, without biasing the shape of the light curve. For the circular aperture photometry, actual co-addition of the frames is not required; rather, a weighted average of the fluxes can be used. The PSF fitting, however, fails for weak or nondetections and thus must be performed on co-added frames for which the S/N is above 3.

Using the magnitude rms and χ^2 fits to the reference objects, we determined that the PSF fitting produces the best results. Images where the PSF fitting failed were co-added to bring the OT S/N above 3. To determine how to group the images for co-adding, we calculated the average fluxes of the OT in the 0.72 FWHM aperture in sets of images weighted by the flux error, which is effectively just the sky noise, because of the weak OT signal. We continued to add successive images to a set until the S/N was greater than 3, and then we co-added each set of images, again using the flux errors as weights.

4. RESULTS

The PSF fit magnitudes are listed in Table 1 and shown in Figure 1 with times relative to $t_{\text{tr}0}$ (i.e., $t = t_{\text{obs}} - t_0$, where t_{obs} is the time of the observation, and $t_0 = t_{\text{tr}0}$). We fit a function of the form $f(t) = f_0 t^\alpha$ to the data and find a power-law decline of $\alpha = -0.894^{+0.034}_{-0.033}$, where we have integrated the probability surface, $P(f_0, \alpha)$, over all f_0 and found the most probable α and the corresponding interval containing 68% of the total probability. The reduced χ^2 for the best fit is $\chi^2/\text{dof} = 52.4/(34 - 1) = 1.59$. A single point at $t_{\text{obs}} - t_{\text{tr}0} \sim 2400$ s alone contributes 19.4 to the χ^2 . We checked the PSF fit magnitudes with the aperture magnitudes for this point and found similar results. Further, we inspected the photometry for neighboring objects and did not find any anomalous behavior, although there was a spike in cloud opacity during the effective integration.

Also shown in Figure 1 are the unfiltered RAPTOR data for the OT (Woźniak et al. 2005). We have subtracted 0.21 mag, which represents the systematic zero-point offset we find between the Henden (2005) field calibration and the USNO B1.0 *R*-band magnitudes for our data, from the RAPTOR data.¹⁴ This zero-point shift appears to fully account for the systematic discrepancy between the ROTSE-III and RAPTOR magnitudes, and we assume that the filter responses are close enough that introduction of a color term is not necessary. The best-fit power-law index for the combined ROTSE-III and RAPTOR data is $\alpha = -0.854 \pm 0.014$, with a reduced χ^2/dof of $178.1/(66 - 1) = 2.74$. The ROTSE-III point at $t_{\text{obs}} - t_{\text{tr}0} \sim 2400$ s contributes 28.8 to this χ^2 , and a single RAPTOR point at $t_{\text{obs}} - t_{\text{tr}0} \sim 600$ s adds an additional 46.5. If we remove the three data points differing by more than 3σ from the above fit, the best fit value becomes $\alpha = -0.844 \pm 0.015$ with $\chi^2/\text{dof} = 1.459$.

Using the revised BAT trigger time, $t_{\text{tr}0}$, Chincarini et al. (2005) find a dramatic initial decline in the XRT light curve (LC), which breaks to a slower decline at 329 s. This behavior is not mirrored in the optical, nor are there indications of any differences in the ROTSE-III and RAPTOR data before and

TABLE 1
ROTSE-IIIb OPTICAL PHOTOMETRY OF GRB 050319

t_{start} (s)	t_{end} (s)	Exposure (s)	C_R	σ
164.12.....	169.12	5	15.97	0.14
178.54.....	183.54	5	16.31	0.19
192.86.....	197.86	5	16.18	0.15
207.48.....	212.48	5	16.31	0.16
222.10.....	227.10	5	16.86	0.29
236.42.....	241.42	5	16.22	0.15
250.94.....	270.46	10	16.67	0.36
279.68.....	284.68	5	16.43	0.18
294.20.....	299.20	5	16.62	0.24
308.52.....	328.52	20	16.89	0.13
338.17.....	358.17	20	16.67	0.10
367.72.....	387.72	20	16.79	0.15
396.96.....	446.82	40	16.95	0.15
455.96.....	475.96	20	16.96	0.22
485.81.....	535.16	40	17.10	0.14
544.71.....	564.71	20	17.05	0.18
573.95.....	593.95	20	17.07	0.20
603.81.....	663.81	60	17.44	0.16
672.96.....	732.96	60	17.46	0.20
742.21.....	802.21	60	17.45	0.20
811.56.....	871.56	60	17.78	0.24
881.22.....	941.22	60	17.42	0.16
950.47.....	1080.23	120	18.00	0.20
1089.38.....	1149.38	60	17.93	0.28
1158.84.....	1218.84	60	18.11	0.34
1228.60.....	1288.60	60	17.99	0.31
1297.75.....	1427.11	120	18.29	0.28
1436.97.....	1774.48	300	18.32	0.21
1784.24.....	2052.92	240	18.29	0.29
2062.07.....	2746.86	600	19.50	0.29
2756.52.....	3163.60	360	18.84	0.25
3172.75.....	3719.54	480	18.70	0.15
3728.69.....	4345.86	420	18.72	0.14
4355.22.....	4902.01	480	18.67	0.31

NOTES.— t_{start} and t_{end} give the time since $t_{\text{tr}0}$ (2005 March 19, 09:29:01.44 UT) in the observer frame, “Exposure” is the total open shutter time, and C_R is the unfiltered magnitude calibrated against the *R*-band magnitudes of Henden (2005).

after the X-ray break; the optical LC simply continues the single power-law decline. With $t_0 = t_{\text{tr}0}$, the initial X-ray decline is also the steepest for any of the growing number of *Swift* GRBs. However, Chincarini et al. (2005) find that the X-ray LC is quite similar to that of GRB 050318 if the start time coincides with the later BAT trigger, $t_{\text{tr}1}$. With this convention, the initial decline becomes more shallow and is more typical of other XRT afterglows (for example, see Fig. 1 of Tagliaferri et al. 2005). We therefore investigated the impact of this change in epoch on the optical light curve. Figure 2 shows that the ROTSE-III and RAPTOR data deviate from a simple power-law decline with this choice for the afterglow start time. Woźniak et al. (2005) have analyzed the RAPTOR data using $t_0 = t_{\text{tr}1}$ and found that a broken power-law model gives a more acceptable fit. Fitting a smoothly broken power law of the form

$$f(t) = f_b 2^{1/s} [(t/t_b)^{-s\alpha_1} + (t/t_b)^{-s\alpha_2}]^{-1/s}, \quad (1)$$

with the smoothing parameter fixed at $s = 20$ for a sharp slope transition, the ROTSE-III data give $\alpha_1 = -0.354^{+0.071}_{-0.062}$, $\alpha_2 = -0.788^{+0.054}_{-0.060}$, and a break time $t_b = 281^{+91}_{-69}$ s, with a best-fit

¹⁴ RAPTOR magnitudes from Woźniak et al. (2005) were calibrated using the USNO B1.0 R2 magnitudes; their reference to USNO A2.0 R2 magnitudes is a misprint (W. T. Vestrand 2005, private communication).

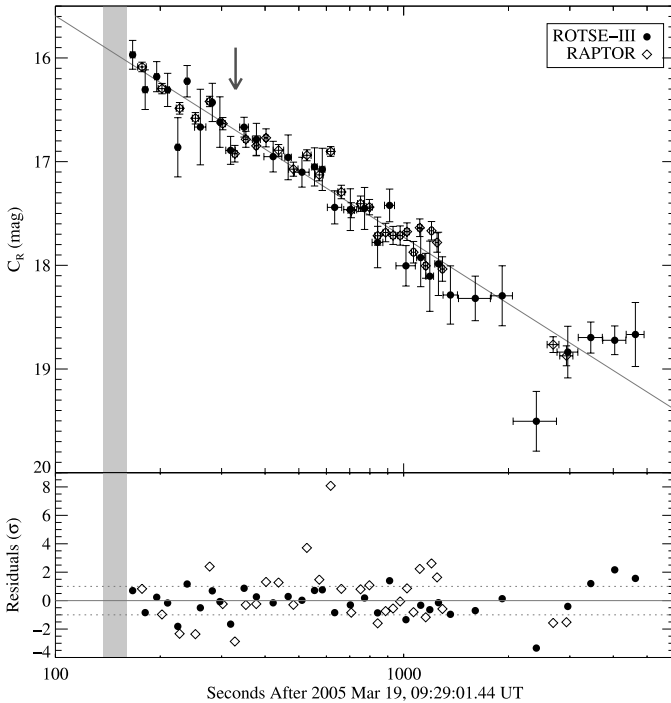


FIG. 1.—ROTSE-III and RAPTOR light curve for the GRB 050319 optical transient for $t_0 = t_{tr0}$. The line gives the best-fit single power law to the combined data set, $\alpha = -0.854$. The vertical shaded band marks the last, FRED-like peak in the γ -ray light curve, and the arrow marks the first break in the XRT light curve. RAPTOR data have been shifted by 0.21 mag as described in the text.

$\chi^2/\text{dof} = 1.57$. A joint fit to the ROTSE-III and RAPTOR data gives $\alpha_1 = -0.364^{+0.020}_{-0.019}$, $\alpha_2 = -0.881^{+0.030}_{-0.031}$, and a break time $t_b = 418^{+31}_{-30}$ s, with a best-fit $\chi^2/\text{dof} = 2.24$. Again, the ROTSE-III and RAPTOR outliers mentioned above add 19.9 and 27.2 to the χ^2 , respectively. Removing the three $>3\sigma$ outliers improves the joint fit to $\alpha_1 = -0.367 \pm 0.022$, $\alpha_2 = -0.864 \pm 0.034$, and a break time $t_b = 405 \pm 40$ s, with a best-fit $\chi^2/\text{dof} = 1.51$.

It is difficult to explain such an early break in the optical LC with the derived decay slopes in the context of the fireball model. One possibility is that energy injection from a long-lived inner engine may be sustaining the optical emission until the break. If so, and assuming that the OT would otherwise have faded as a simple power law with $\alpha = \alpha_2$ from the first ROTSE-III point, then the energy injected from $t_{\text{obs}} - t_{\text{tr1}} = 30$ s to t_b increased the postbreak optical flux by 3.9 times.

We have also considered the possibility that the break is due to a synchrotron break. For example, if we naively assume the prebreak data were taken around the time when the typical electron synchrotron frequency, ν_m , drops below our observing range, then the observed α_1 could be the typical $-1/4$ index for fast cooling and a constant-density ISM diluted by the transition to the steeper decline. However, for the later decline we should have $\alpha_2 = -(3p - 2)/4$, which results in $p = 1.84$, an unusual value for the electron power-law index (note that when $p < 2$, there is an imposed maximum in the distribution of electron Lorentz factors, which will alter the relation of p and α). There is not a fixed value for p that predicts both α_1 and α_2 using the relations for slow cooling with $1 < p < 2$ derived in Dai & Cheng (2001). Other synchrotron breaks, such as the cooling break, result in similarly atypical values for p . Furthermore, the X-ray LC breaks to a more shallow decline instead of the switch to a steeper decline found in the optical at close to the same time, which is not commensurate with a synchrotron

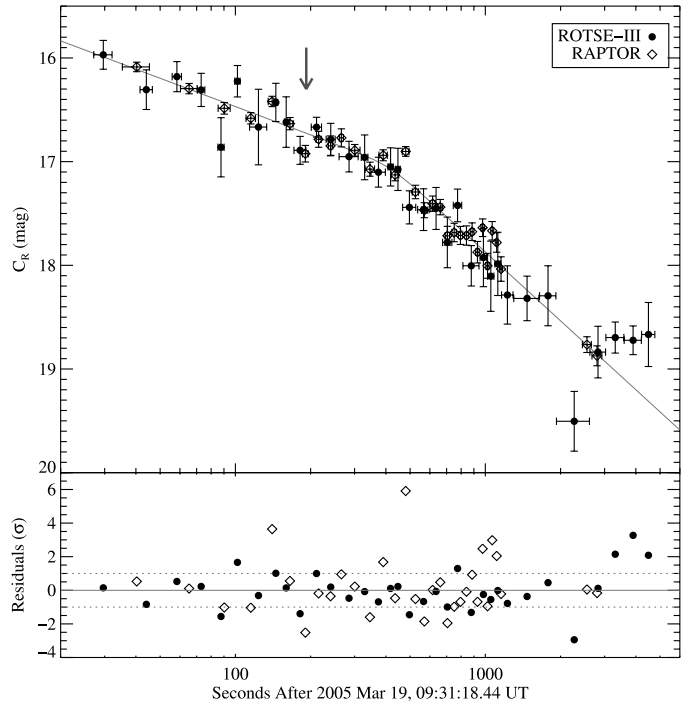


FIG. 2.—ROTSE-III and RAPTOR light curve for the GRB 050319 optical transient for $t_0 = t_{tr1}$. The line gives the best smoothly broken power-law fit to the joint data set with $\alpha_1 = -0.36$, $\alpha_2 = -0.88$, and $t_b = 418$ s. The smoothness parameter was fixed at $s = 20$. The arrow marks the first break in the XRT light curve.

break. The break is also not explained by a jet break, since it is not achromatic.

5. DISCUSSION

The afterglow of GRB 050319 may have begun at the first of two strong γ -ray peaks with the steepest decline in the X-ray of any of the GRBs captured by *Swift*, and showed no correlated behavior in its optical LC; or perhaps it began at the last peak in the γ -rays and had a normal X-ray LC and an optical LC, with a break around 300 s between unusual power-law decline indices. In either case, there is no correlation between the X-ray and optical light curves: the X-ray LC breaks do not coincide with optical breaks, and the X-ray decline rates do not match the optical slopes. The decline mismatch means that the X-ray to optical color is continually changing, and the spectral slope β (where $f_\nu \propto \nu^\beta$) is not a constant from the X-ray to the optical.

In the context of the fireball model, reverse-shock emission has been predicted to dominate the early afterglow, giving a steep initial decline (Sari & Piran 1999). Reverse-shock emission has been used to explain the initial rapid optical decline of the GRB 990123 afterglow, and may account for the steep decline in the early XRT light curve for GRB 050319; however, this emission is expected to peak in the optical or infrared, and no such signal is observed in the contemporaneous optical data. Tagliaferri et al. (2005) and Kobayashi et al. (2005), however, have discussed suppression of the optical signal through inverse Compton scattering. In this case the optical photons produced in the reverse shock are upscattered, which creates the fast-decaying X-ray signal. Kobayashi et al. (2005) show that while inverse Compton effects can highly suppress optical emission in the reverse shock, inverse Compton emission can be less important in the forward shock. Upscattering of the reverse shock optical emission could help explain why there is no change in the optical decay during the first break in the X-ray LC. However, Cusumano et al.

(2006) suggest that the initial fast X-ray decay may represent the low-energy tail from the prompt emission, in which case no reverse-shock emission was observed in any band.

The true behavior of the optical light curve is critically dependent on the choice of t_0 . In general, for accurate analysis the error in t_0 must be much less than the epochs in which power laws are to be evaluated. Although the reduced χ^2 is smaller for the smoothly broken power-law fit to the combined ROTSE-III and RAPTOR data with $t_0 = t_{tr1}$ than for the single power-law fit to the same data with $t_0 = t_{tr0}$ (including the outliers in both cases), neither model can acceptably account for the scatter shown in the sample. If such fluctuations are intrinsic to early OT light curves, it will be difficult to use statistical arguments to determine the starting time, t_0 , through fits to simple power-law functions. The behavior predicted by the fits for the two choices of t_0 we consider differ by about 0.2 mag from published magnitude estimates during later times, although the errors for the two models overlap. Woźniak et al. (2005) have shown using data from the GCN Circulars that the decay rate of the OT appears to slow after 1.3 hr, and as a result we cannot use predictions for the late-time behavior from the single and smoothly broken power-law fits of the early-time data to constrain t_0 .

If the optical emission began during the first peak in the γ -rays, then there are no deviations from a simple power law in the early phases that can be attributed to the last γ -ray peak, even though the ROTSE-III data begin 27 s after the last peak and just 4 s after the cessation of γ -ray activity. Therefore, this scenario leads to a physical difference in the first γ -ray peak, which is followed by long-lived optical emission, and the last γ -ray peak, which has no detected optical emission and at most optical emission several times fainter than that associated with the first peak.

As the GRB 050319 OT clearly illustrates, shifting t_0 to a later time can turn a simple power law into an apparent broken power law. Because this shift, $t'_0 = t_0 + \Delta t$, makes the logarithmic difference between two epochs larger while the drop in flux remains the same, the early light curve ($t' < \Delta t$) appears to flatten out, and we infer $\alpha'_1 \approx 0$. For $t' \gg \Delta t$ the effect is negligible, and we have $\alpha'_2 \approx \alpha$. Setting $\alpha_1 = 0$, $\alpha_1 = \alpha$, and $s = -1/\alpha$ into equation (1) gives $f(t) = f'_0(t + t_b)^\alpha$, which is identical to a single power law shifted by t_b . However, a broken power law with a sharp transition ($s \gg -1/\alpha_2$) can be distinguished from a single power law with an incorrect t_0 if the light curve is well sampled and the error bars are ~ 0.1 mag or smaller, which ROTSE-III can deliver. It is therefore possible at least to determine whether an apparent early light curve break is due

to an error in the adopted t_0 even for $\alpha_1 \approx 0$ if the transition is sharp. There are events that exhibit just such behavior, such as the optical transient to GRB 050801 (Rykoff et al. 2006).

It is important to note that γ -ray burst triggers are defined by instrument response and software algorithms and do not necessarily mark the start of the burst itself, much less the afterglow. There are many examples in which the γ -ray emission is detected prior to the formal trigger. For example, GRB 050915B showed γ -ray activity 10 s prior to the formal trigger (Falcone et al. 2005), while emission began at least 8 s before the GRB 050908 trigger (Sato et al. 2005), and GRB 050827 started 15 s before its trigger (Sakamoto et al. 2005). Lazzati (2005) searched BATSE data in the range $-200 \text{ s} < t < t_{tr}$ and found that about 20% of bursts showed evidence for precursor activity. Setting t_0 to the precursor time would effectively steepen the observed afterglow decline rate and could thus lead to a different interpretation of the LC, such as the presence of reverse-shock emission. There have also been bright bursts like GRB 990123 that began with ~ 15 s of weak γ -ray emission and later showed bright peaks (Briggs et al. 1999). Assuming a similar light curve behavior for weaker bursts, the trigger time could be delayed in some cases. The derived decline rate based on the trigger would then be slower than the decline rate based on the true start of the burst, and the shift could introduce an apparent break in the observed afterglow LC.

The extended and highly variable nature of long-duration GRBs suggests that the afterglow itself may not begin cleanly from a given epoch, but rather we might expect a turn-on phase in which energy injection drives the optical emission and perhaps produces a highly variable light curve similar to that of GRB 050319, with $t_0 = t_{tr1}$. However if t_{tr0} did mark the start of the afterglow, then the lack of a bulk departure from the simple power-law decline as a result of energy injection related to the last γ -ray peak argues against a γ -ray/optical correlation. As *Swift* continues to provide prompt GRB locations, it becomes more important to answer the question, “when does the afterglow begin?” in order to correctly interpret the light curves.

This work has been supported by NASA grants NNG-04WC41G and F006794, NSF grants AST 01-19685 and 0105221, the Australian Research Council, the University of New South Wales, and the University of Michigan. Work performed at LANL is supported through internal LDRD funding. Special thanks to the observatory staff at McDonald Observatory, especially David Doss.

REFERENCES

- Akerlof, C. W., et al. 2003, *PASP*, 115, 132
 Bertin, E., & Arnouts, S. 1996, *A&AS*, 117, 393
 Briggs, M. S., et al. 1999, *ApJ*, 524, 82
 Chincarini, G., et al. 2005, *ApJ*, submitted (astro-ph/0506453)
 Cusumano, G., et al. 2006, *ApJ*, 639, 316
 Dai, Z. G., & Cheng, K. S. 2001, *ApJ*, 558, L109
 Falcone, A., et al. 2005, *GCN Circ.*, 3987, 1
 Fynbo, J. P. U., et al. 2005, *GCN Circ.*, 3136, 1
 Henden, A. 2005, *GCN Circ.*, 3454, 1
 Kobayashi, S., et al. 2005, preprint (astro-ph/0506157)
 Krimm, H., et al. 2005, *GCN Circ.*, 3117, 1
 Landsman, W. B. 1989, *BAAS*, 21, 784
 Lazzati, D. 2005, *MNRAS*, 357, 722
 Rykoff, E., Schaefer, B., & Quimby, R. 2005, *GCN Circ.*, 3116, 1
 Rykoff, E. S., et al. 2006, *ApJ*, 638, L5
 Sakamoto, T., et al. 2005, *GCN Circ.*, 3894, 1
 Sari, R., & Piran, T. 1999, *ApJ*, 520, 641
 Sato, G., et al. 2005, *GCN Circ.*, 3951, 1
 Stetson, P. B. 1987, *PASP*, 99, 191
 Tagliaferri, G., et al. 2005, *Nature*, 436, 985
 Woźniak, P. R., et al. 2005, *ApJ*, 627, L13